Structure of the Prolidase from *Pyrococcus furiosus*†

Megan J. Maher,‡ Mousumi Ghosh,§,# Amy M. Grunden,§,⊥ Angeli L. Menon,§ Michael W. W. Adams,§ Hans C. Freeman,*,‡ and J. Mitchell Guss*,‡

School of Molecular and Microbial Biosciences, University of Sydney, New South Wales 2006, Australia, and Department of Biochemistry and Molecular Biology and Center for Metalloenzyme Studies, University of Georgia, Athens, Georgia 30602 USA

Received September 12, 2003; Revised Manuscript Received December 12, 2003

ABSTRACT: The structure of prolidase from the hyperthermophilic archaeon *Pyrococcus furiosus* (*Pf*prol) has been solved and refined at 2.0 Å resolution. This is the first structure of a prolidase, i.e., a peptidase specific for dipeptides having proline as the second residue. The asymmetric unit of the crystals contains a homodimer of the enzyme. Each of the two protein subunits has two domains. The C-terminal domain includes the catalytic site, which is centered on a dinuclear metal cluster. In the as-isolated form of *Pf*prol, the active-site metal atoms are Co(II) [Ghosh, M., et al. (1998) *J. Bacteriol. 180,* 4781−9]. An unexpected finding is that in the crystalline enzyme the active-site metal atoms are Zn(II), presumably as a result of metal exchange during crystallization. Both of the Zn(II) atoms are five-coordinate. The ligands include a bridging water molecule or hydroxide ion, which is likely to act as a nucleophile in the catalytic reaction. The two-domain polypeptide fold of *Pf*prol is similar to the folds of two functionally related enzymes, aminopeptidase P (APPro) and creatinase. In addition, the catalytic C-terminal domain of *Pf*prol has a polypeptide fold resembling that of the sole domain of a fourth enzyme, methionine aminopeptidase (MetAP). The active sites of APPro and MetAP, like that of *Pf*prol, include a dinuclear metal center. The metal ligands in the three enzymes are homologous. Comparisons with the molecular structures of APPro and MetAP suggest how *Pf*prol discriminates against oligopeptides and in favor of Xaa−Pro substrates. The crystal structure of *Pf*prol was solved by multiple-wavelength anomalous dispersion. The crystals yielded diffraction data of relatively high quality and resolution, despite the fact that one of the two protein subunits in the asymmetric unit was found to be significantly disordered. The final R and R_{free} values are 0.24 and 0.28, respectively.

Prolidases are peptidases with a preference for Xaa−Pro dipeptide substrates. Enzymes of this type have been isolated from mammals (*1*−*3*), bacteria (*Lactobacillus* (*4*) and *Xanthomonas* (*5*)), and an archeon (*Pyrococcus* (*6*)). In humans, prolidase is involved in the final stage of the degradation of endogenous and dietary proteins, and is particularly important in collagen catabolism. Mutations in the gene encoding for human prolidase cause prolidase deficiency, an autosomal recessive disorder characterized by skin lesions, mental retardation, and recurrent infections (*7*, *8*). The physiological role of the enzyme in bacteria and archaea is unclear. In general, proline-specific peptidases participate with other endo- and exo-peptidases in the terminal degradation of intracellular proteins, and may function in the recycling of proline.

In addition to its fundamental interest as an example of peptidase specificity, prolidase has biotechnological applications. The enzyme has a potential use in the dairy industry as a cheese-ripening agent, since the release of proline from peptides in cheese reduces bitterness (*9*). Further, an enzyme originally described as organophosphorus acid anhydrolase (OPAA),[1] is actually a prolidase (*10*). The OPAA from *Alteromonas* sp. strain JD6.5 has 22% sequence identity with human prolidase, and—like human prolidase—catalyzes the

† Support from the Australian Research Council (DP0209273) to J.M.G. and H.C.F., and from the U.S. Department of Energy (FG05-95ER20175) and the National Science Foundation (MCB 0129841) to M.W.W.A. M.J.M. is an Australian Research Council Postdoctoral Fellow. Access to the facilities of the Stanford Synchrotron Radiation Laboratory (SSRL) was supported by a travel grant from the Access to Major Research Facilities Program administered by the Australian Nuclear Science and Technology Organization. The SSRL Structural Molecular Biology Program is supported by the Department of Energy, Office of Biological and Environmental Research, and the National Institutes of Health, National Center for Research Resources, Biomedical Technology Program, and the National Institute of General Medical Sciences.

* To whom correspondence should be addressed. (H.C.F.) Tel: +61 (0)2 9351 4405. Fax: +61 (0)2 9351 4726. E-mail: freemanh@chem.usyd.edu.au. (J.M.G.) Tel: +61 (0)2 9351 4302. Fax: +61 (0)2 9351 4726. E-mail: m.guss@mmb.usyd.edu.au.

‡ University of Sydney.

§ University of Georgia.

⊥ Present address: Department of Microbiology, North Carolina State University, Raleigh, NC 27695, USA.

Present address: Department of Pharmacology and Physiology, University of Rochester, Rochester, NY 14642, USA.

[1] Abbreviations: AHMH-Pro, (2*S*,3*R*)-3-amino-2-hydroxy-5-methylhexanoyl-proline; *Ap*AP, aminopeptidase from *Aeromonas proteolytica*; CPG_2, carboxypeptidase G_2 from *Pseudomonas* sp. strain RS-16; *Ec*APPro, X-Pro aminopeptidase, aminopeptidase P from *Escherichia coli*; bLeuAP, leucine aminopeptidase from bovine lens; *Hs*MetAP, human methionine aminopeptidase-2; MAD, multiple wavelength anomalous dispersion; *Ec*MetAP, methionine aminopeptidase from *Escherichia coli*; MPD, 2-methyl-2,4-pentanediol; OPAA, organophosphorus acid anhydrolase; PEG, poly(ethylene glycol); *Pf*MetAP, methionine aminopeptidase-2 from *Pyrococcus furiosus*; *Pf*prol, prolidase, X-Pro dipeptidase from *Pyrococcus furiosus*; rmsd, root-mean-square distance; *Sg*AP, aminopeptidase from *Streptomyces griseus*.

10.1021/bi0356451 CCC: $27.50
Published on Web 02/14/2004

hydrolysis of Xaa−Pro dipeptides when activated by Mn^{2+} ions. However, in contrast with human prolidase, OPAA can hydrolyze not only dipeptides but also organophosphorus acetylcholinesterase inhibitors. The latter are highly toxic, and can be used as pesticides and chemical warfare agents. It is likely that OPAA has a natural function in peptide metabolism rather than detoxification (*10*).

The prolidase from the hyperthermophilic archaeon *Pyrococcus furiosus* (*Pf*prol) has been isolated and characterized, and the recombinant form of the enzyme has been obtained from *Escherichia coli* (*6*). The enzyme is a homodimer with a subunit molecular mass of 39.4 kDa. When purified from either *P. furiosus* or *E. coli*, *Pf*prol contains only one Co(II) atom per subunit. Full catalytic activity requires the addition of Co^{2+} ions, indicating that the enzyme has a second metal-binding site. In the assay, Co^{2+} can be replaced by Mn^{2+}, but not by Mg^{2+}, Ca^{2+}, Fe^{2+}, Zn^{2+}, Cu^{2+}, or Ni^{2+} (*6*). *Pf*prol has a narrow substrate specificity, hydrolyzing only dipeptides Xaa−Pro, where Xaa is nonpolar (Met, Leu, Val, Phe, Ala). Optimal activity with Met−Pro as the substrate occurs at pH 7.0 and a temperature of 100 °C (*6*). The protein used in the present work was a recombinant form of *Pf*prol, whose molecular mass, metal-ion dependence, pH and temperature optima, substrate specificity, and thermal stability are indistinguishable from those of the native enzyme.

A recent review of metallopeptidase properties (*11*) classifies *Pf*prol in a subclass of metallopeptidases with dinuclear active-site metal clusters. Members of the subclass that have previously been characterized crystallographically are *E. coli* methionine aminopeptidase (MetAP) (*12*), *E. coli* proline aminopeptidase (APPro) (*13*), bovine lens leucine aminopeptidase (*b*LeuAP) (*14*), *Aeromonas proteolytica* aminopeptidase (*Ap*AP) (*15*), *Streptomyces griseus* aminopeptidase (*Sg*AP) (*16*), human methionine aminopeptidase-2 (*Hs*MetAP) (*17*), *Pyrococcus furiosus* methionine aminopeptidase-2 (*Pf*MetAP) (*18*), and carboxypeptidase G_2 from *Pseudomonas* sp. strain RS-16 (*19*). What these enzymes have in common is a dinuclear metal cluster bridged by a hydroxide ion. The metal cluster promotes catalysis by providing a site for substrate binding, by activating a nucleophile for the reaction, and presumably by stabilizing the transition state. In some cases, full activity depends on the presence of two metal atoms at the active site. In others, only a single metal atom is required for catalysis, and binding of the second metal ion modulates activity either positively or negatively. The metal found at the active site of an as-isolated enzyme is seldom unique in supporting catalytic activity, and the metal that is used by the enzyme in vivo is frequently hard to identify.

Strong structural homologies among some of the proteins cited above have been recognized. For example, the polypeptide folds of the catalytic domains of APPro and MetAP are closely similar, and the dinuclear metal clusters in the two enzymes are coordinated by identical sets of residues (*11*). In the crystal structures of MetAP and APPro, the active-site metal atoms are Co(II) and Mn(II), respectively.

We report here the crystal structure of *P. furiosus* prolidase in which the naturally occurring Co(II) atoms have been replaced by Zn(II). Strong structural homologies with APPro and MetAP are observed. Comparisons among the three molecular structures then suggest how *Pf*prol discriminates against oligopeptides and in favor of Xaa−Pro dipeptide substrates.

Chart 1. The Inhibitor (2*S*,3*R*)-3-Amino-2-hydroxy-5-methyl-hexanoyl-proline (AHMH-Pro).

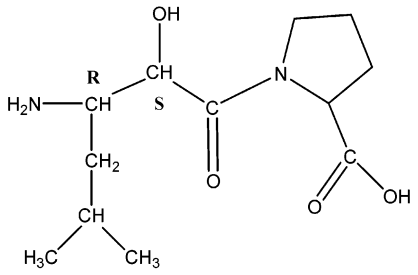

EXPERIMENTAL PROCEDURES

Purification, Crystallization, and Data Collection. The gene encoding *Pf*prol was expressed in *E. coli* and the recombinant enzyme was purified as described previously (*6*). Crystals of *Pf*prol were grown by vapor diffusion at 20 °C and were obtained after approximately 180 days (*20*). Hanging drops containing protein (2.5 μL, 10 mg/mL), PEG 8K (6.5−7.5%), magnesium acetate (0.1 M), and Tris-HCl buffer (50 mM, pH 8.5) were equilibrated against a reservoir (1.0 mL) containing PEG 8K (13−15%) and magnesium acetate (0.2 M) in the same buffer. The crystals belonged to space group $P2_1$ with the following unit cell parameters: $a = 56.5$, $b = 97.3$, $c = 70.0$ Å, $\beta = 97.1°$. These parameters identified the crystals as the previously reported "form II" (*20*). Reasonable values for the crystal density suggested that there are two monomers in the asymmetric unit. Crystals were cryoprotected by replacing the mother liquor with mixtures of the reservoir solution containing increasing concentrations of 2-methyl-2,4-pentanediol (MPD), and were then transferred rapidly into a cold N_2 gas stream.

High-resolution (2.0 Å) multiple-wavelength anomalous dispersion data were collected from a single frozen crystal on beamline 9-2 at the Stanford Synchrotron Radiation Laboratory, using an ADSC Q4 CCD detector. A broad X-ray excitation scan of the crystal gave an intense absorption edge at 9665 eV, characteristic of the presence of Zn. Preliminary data collection was carried out at the peak absorption energy (λ_1, 1.282 Å, 9674 eV). An anomalous Patterson map calculated during data collection showed strong peaks, indicating that the Zn atoms were located in ordered sites. Additional data were collected at four wavelengths near the Zn absorption edge, using the reverse-beam technique: λ_1, 1.282 Å, 9674 eV (the f'' peak); λ_2, 1.283 Å, 9665 eV (the inflection point); λ_3, 1.240 Å, 10 000 eV (a high energy remote from the absorption edge); and λ_4, 1.333 Å, 9300 eV (a low energy remote from the absorption edge). For the preparation of an inhibitor complex, a single crystal was soaked (1 h) in reservoir solution containing a small amount of solid (2*S*,3*R*)-3-amino-2-hydroxy-5-methyl-hexanoyl-proline (AHMH-Pro) (Chart 1) and MPD (15%), before being frozen in the cold gas stream. Data were collected to 2.3 Å resolution at 110 K on an R-AXIS IIc image-plate detector with Cu Kα X-rays from a Rigaku RU-200 rotating-anode generator focused using mirror optics. The unit-cell parameters were closely similar to those of the native crystals (Table 1a). The diffraction data were pro-

Table 1: (a) Crystallographic Data and (b) Refinement Statistics for *Pf*prol and Its AHMH Complex

(a) Crystallographic Data

protein	native λ_1	native λ_2	native λ_3	native λ_4	inhibitor complex
X-ray wavelength (Å)	1.282	1.283	1.240	1.333	1.5418
temperature (K)			100		113
space group			$P2_1$		$P2_1$
unit-cell parameters					
a (Å)			56.5		56.6
b (Å)			97.3		97.0
c (Å)			70.0		69.8
β (°)			97.1		97.0
resolution (Å)	2.0	2.0	2.0	2.05	2.30
unique observations[a]	48181	48237	48104	43401	28950
total observations[b]	181495	182604	182841	204555	42006
completeness (%)[c]	95.3 (97.7)	95.4 (97.5)	95.1 (97.5)	91.6 (92.8)	88.0 (87.5)
$I/\sigma(I)$[c]	28.8 (4.4)	28.3 (3.7)	28.3 (3.7)	42.9 (3.5)	9.2 (3.1)
R_{merge}[d]	0.039 (0.225)	0.032 (0.285)	0.034 (0.287)	0.027 (0.335)	0.057 (0.192)
figure of merit[e]			0.616		

(b) Refinement Statistics

protein	native protein	inhibitor complex
X-ray wavelength (Å)	1.240 (λ_3)	1.5418
resolution range (Å)	20.0−2.0	20.0−2.3
residues included in model	A8−A106, A108−A345 B4−B226, B244−B275, B277−B296, B299−B317, B322−B345	A8−A15, A19−A106, A108−A345 B4−B201, B203−B226, B244−B265, B268−B275, B277−B297, B299−317, B322−345
total no. of protein residues	655	648
no. of protein residues, subunit A	337	334
no. of protein residues, subunit B	318	314
no. of Zn atoms	4	4
no. of water molecules	176	118
no. of other entities		1 (AHMH-Pro)
total no. of atoms	5376	5101
reflections	48099	28946
R_{cryst}[f]	0.24	0.25
R_{free}[f,g]	0.28	0.33
rms Δ − bond lengths (Å)	0.005	0.017
rms Δ − bond angles (°)	0.8	2.0
average B-value (Å^2)	22	28
ESU (Å)[h]	0.2	0.3

[a] Friedel pairs are counted as a single unique observation. [b] Friedel pairs are counted separately in the total number of observations. [c] Values in parentheses are for the highest resolution shell. [d] $R_{merge} = \sum|I_h - \langle I_h\rangle|/\sum\langle I_h\rangle$. [e] Figure of merit was obtained from the program MLPHARE for 20−2 Å resolution. [f] *R* values $= \sum|F_{obs} - F_{calc}|/\sum F_{obs}$. [g] 5% of the reflections were reserved for calculation of R_{free}. [h] Estimated standard uncertainty, calculated as the diffraction data precision indicator (*46*).

cessed using programs DENZO and SCALEPACK (*21*). Data collection statistics are summarized in Table 1a.

Structure Determination and Refinement. The 2.0 Å resolution structure of *Pf*prol was solved by MAD at the Zn absorption edge. The positions of four Zn atoms were determined using CNS (*22*). MLPHARE (*23*) was used for refinement of the Zn coordinates and to calculate initial phases to 2.0 Å resolution. Solvent flattening with histogram matching using DM was used to improve the phases (*23*, *24*). The best electron-density maps were obtained when λ_2 (Table 1a) was used as the reference wavelength. The electron density was readily interpretable, and indicated that a dimer of *Pf*prol was present in the asymmetric unit. An initial model of half of the dimer, "subunit A", could be built, using the program O (*25*). Subunit A was then superposed on the electron density of the other half of the dimer, "subunit B", and manual adjustments to the model were made in O. At this stage, it was already apparent that the electron density for molecule A was defined much better than that for molecule B. The model of the dimer was initially refined using CNS with iterative cycles of simulated annealing, individual *B*-value, and positional refinement, followed by model building using O. The refinement to 2.0 Å resolution was completed with the data recorded at the highest energy, λ_3 (Table 1a), using REFMAC5 with TLS (*26*). For the structure analysis of the complex with the inhibitor AHMH-Pro, a molecule of AHMH-Pro was oriented manually in difference electron density at the active site of monomer A. Refinement was then carried out using REFMAC5 with TLS. Coordinates and structure amplitudes for the structure of *Pyrococcus furiosus* prolidase have been deposited at the PDB with the accession code 1PV9.

Analytical Methods. The concentrations of zinc and cobalt in the crystallization solutions were determined by plasma emission spectroscopy with a Jarrel Ash Plasma Comp 750 Instrument.

RESULTS

The Metal Content of Pfprol Crystals. Since native *Pf*prol requires two active site Co atoms per molecule for full

activity (*6*), we intended to record the requisite diffraction data at several wavelengths near the cobalt X-ray absorption edge. Surprisingly, X-ray fluorescence scans of the crystals failed to produce any sign of a Co signal. Instead, the crystals had a strong absorption edge corresponding to Zn. When data recorded at wavelengths near the Zn X-ray absorption edge were used in the MAD structure analysis, four Zn atoms per asymmetric unit (see below) were located immediately and unequivocally. It therefore seemed that the active site Co atoms had been replaced by Zn during the long crystallization process. An analysis of the reservoir solution against which the hanging drops had been equilibrated—and which had formed 50% of the each hanging drop—confirmed a high concentration of Zn^{2+} (140 μM) but only a trace of Co^{2+} (0.2 μM). Moreover, analysis of dissolved crystals revealed a protein/Co/Zn ratio of approximately 1:1:165, consistent with the X-ray absorption edge. The specific activity of the enzyme obtained from the crystals (590 U/mg, determined under standard assay conditions at 100 °C in the presence of 1.2 mM Co^{2+}; ref *6*) was about 50% of that (1300 U/mg) of enzyme that had not been crystallized. Thus, the Zn ions at the active site of the enzyme are readily displaced by Co under the assay conditions. In any event, the protein that did crystallize had indeed been exposed to a significant amount of Zn^{2+} as an impurity in the crystallization medium, and this led to an exchange of active site cobalt for zinc during crystallization.

Molecular Structure. The refinement of the *Pf*prol structure using the data recorded from the native crystal converged with residuals $R = 0.24$ and $R_{free} = 0.28$ (Table 1b). The asymmetric unit contains a single homodimer. Consistent with electron-density maps throughout the refinement, subunit A is well defined, while subunit B is significantly disordered. Altogether, the refined model has 655 protein residues, 176 water molecules, and 4 Zn atoms (Table 1b). The model of subunit A comprises residues 8−106 and 108−345, i.e., 337 of the 348 residues in the complete amino acid sequence. All these residues were represented by excellent electron density, and refined to an average temperature factor $B = 22$ Å^2. The only exceptions occurred at residue Asn 107 and at one or more atoms in 33 side chains, which were in weak electron density and were assigned zero occupancy. In subunit B, only 318 residues could be modeled and refined successfully. Four sections of the polypeptide chain were not located in significant electron density, and were omitted from the final model (Table 1b). In addition, parts of 36 side chains were assigned zero occupancy since the refinement consistently produced unacceptably high-temperature factors (60−100 Å^2). The disorder in parts of the protein molecules extends into the solvent. There are only 176 ordered water molecules in the model, corresponding to <0.3 water per amino acid.

The molecular structure of *Pf*prol is best described using subunit A, since this is well defined. The polypeptide fold is shown in Figure 1. The subunit has an N-terminal domain (domain I, residues 1−112), an α-helical linker (residues 113−123), and a C-terminal domain (domain II, residues 124−348). Domain I consists of a six-stranded mixed β-sheet flanked by five α-helices (three on one side and two on the other). Domain II is formed around a mixed six-stranded β-sheet with four α-helices on the outer surface. The β-sheet is so strongly curved that it has a "pita-bread" fold. The only direct contacts between the domains are hydrogen bonds between the end of a small helix in domain I (residues 24−32) and a β-turn in domain II (residues 284−294). The tertiary structure is further stabilized by hydrogen bonds from Arg122 in the linker helix to Gln27 in domain I and to Glu289 and Glu292 in domain II. There is also a weak $\pi-\pi$ interaction between the side chains of Tyr29 in domain I and His216 in domain II (ring−ring separation 3.6 Å). Details of the contacts between the domains have been deposited as Supporting Information.

The *Pf*prol dimer (Figure 2) has approximate dimensions 51 × 67 × 53 Å. It is held together by a relatively small number of contacts between the two monomers. Since the dimer has approximate (noncrystallographic) 2-fold symmetry, it is not surprising that the contacts occur between equivalent residues in the subunits. Residues A92−A97 form a short segment of antiparallel β-sheet with residues B92−B97, and residues A158−A172 in a helix are hydrogen-bonded to the equivalent residues B158−B172 (Supporting Information). Approximately 10% (1525 Å^2) of the surface area of each subunit is buried as a result of dimer formation. The extent of the buried surface is "moderate" according to a recent survey of 28 homodimer structures (*27*).

Active Site. The active site (Figure 3) is located in an oval depression on the inner (concave) surface of the curved β-sheet of domain II. Its central feature is a dinuclear Zn cluster. The Zn atoms are coordinated by the side chains of two aspartate residues (Asp209 and Asp220), two glutamate residues (Glu313 and Glu327), a histidine (His284), and a bridging atom modeled as water (W176). The carboxylate groups of Asp220 and Glu327 act as bridges between the Zn atoms. The Zn−ligand distances are listed in Table 2.

Each Zn atom has an approximately trigonal−bipyramidal coordination geometry. Zn_A is coordinated by $O^{\delta 2}$(Asp220), $N^{\epsilon 2}$(His284), and $O^{\epsilon 2}$(Glu327) in the equatorial plane, and by W176 and $O^{\epsilon 2}$(Glu313) on the axis. The coordination sphere of Zn_B comprises $O^{\delta 1}$(Asp209), $O^{\delta 2}$(Asp209), $O^{\delta 1}$(Asp220), $O^{\epsilon 1}$(Glu327), and W176 (Table 2). The side chain of Asp209 acts as an unsymmetrical bidentate ligand with Zn_B-O^{δ} distances of 2.1 and 2.8 Å, respectively (Table 2).

A Prolidase−Inhibitor Complex. Crystals of prolidase that had been soaked in a solution of the inhibitor AHMH-Pro, (2*S*,3*R*)-3-amino-2-hydroxy-5-methyl-hexanoyl-l-proline, yielded diffraction data of lower quality than crystals of the native protein (Table 1a). AHMH-Pro resembles the natural product "bestatin", *N*-[(2*S*,3*R*)-(3-amino-2-hydroxy-1oxo-4-phenylbutyl]-L-leucine, which is a known inhibitor of aminopeptidases (*28*). Preliminary refinement indicated that, as found in the native protein, substantial segments of molecule B were disordered. Refinement of the structure resulted in a model with $R = 0.25$ and $R_{free} = 0.33$. Electron-density ($F_{obs} - F_{cals}$) maps consistently showed significant residual density within the active site pocket of subunit A (Figure 4). There was no equivalent difference electron density in the active site of subunit B.

The interaction between prolidase and AHMH-Pro causes no gross structural rearrangement. The rmsd between the positions of 648 equivalent C^{α} atoms in the native and inhibitor-complexed proteins is 0.3 Å. The AHMH-Pro molecule is bound at the active site of subunit A, where it interacts with both Zn atoms. The terminal N(amino) atom

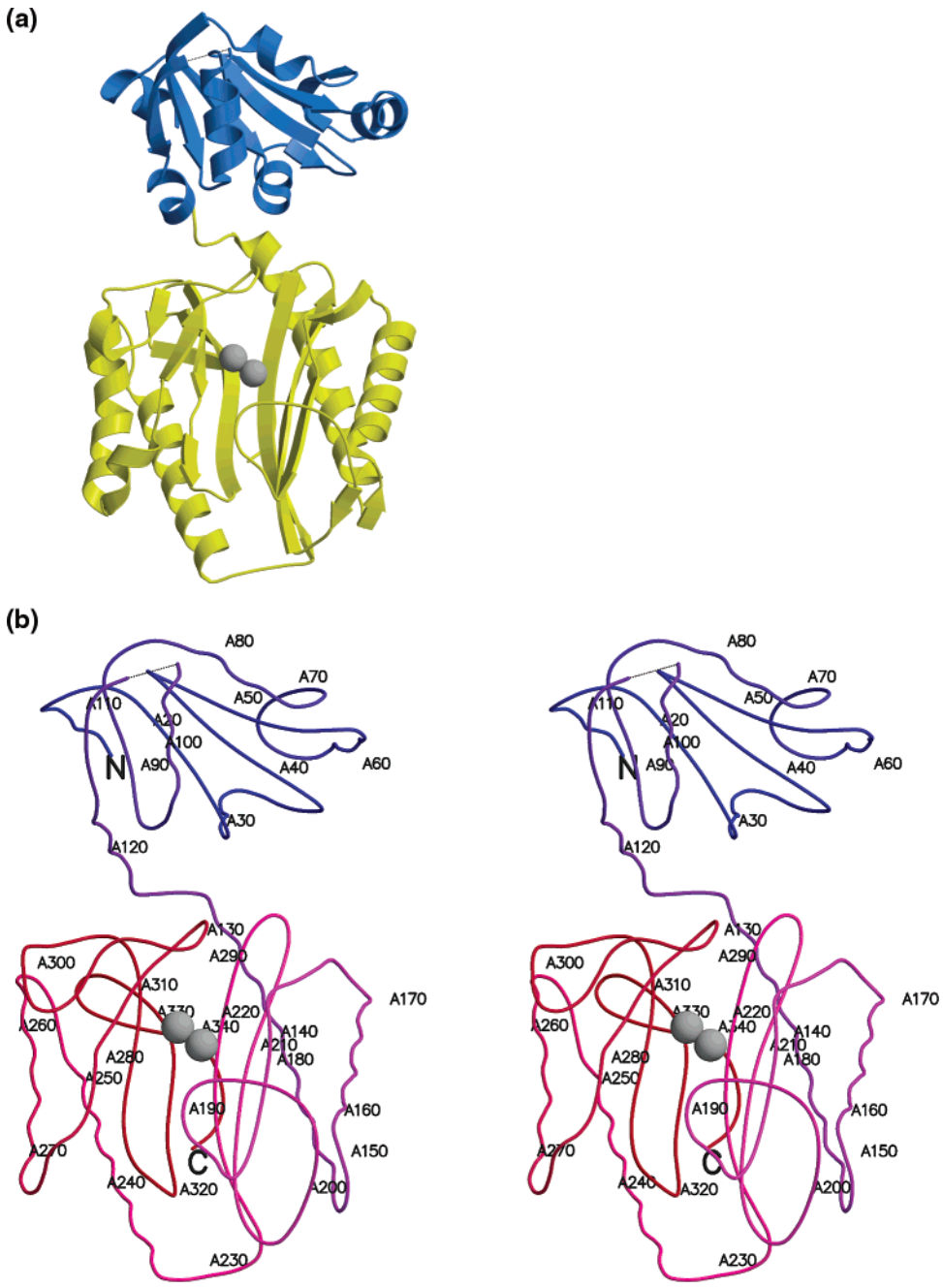

FIGURE 1: The structure of a monomer of *Pf*prol. (a) Ribbon drawing highlighting the domain structure; N-terminal domain is in blue and the C-terminal domain is yellow. The Zn atoms are shown as gray spheres. (b) Stereoview of the backbone trace in the same orientation as (a), ramp colored from blue to red with every tenth residue numbered. The missing residue 107 is shown as a dashed line. The N- and C-termini are marked. Figures 1, 2, 3, 4b, 5 and 6 were drawn with programs MOLSCRIPT (*48*) and RENDER (*49*).

of the inhibitor becomes an axial ligand of Zn_B (Zn_B-N = 1.9 Å), and the O(hydroxyl) atom bridges Zn_A and Zn_B ($Zn_A-O2 = Zn_B-O2$ = 2.2 Å) (Table 2). Electron−density maps indicated that the inhibitor displaces the carboxylate group of Glu313 from the coordination sphere of Zn_A. No electron density was observed for the side chain of Glu 313.

DISCUSSION

The Metal Site in Prolidase: A Cautionary Tale. The finding that *Pf*prol crystals lacked significant amounts of Co and instead contained Zn has some valuable lessons and emphasizes that the nature of the metal atoms in a metalloprotein crystal structure cannot be taken for granted. When isolated, *Pf*prol contains one Co(II) atom per molecule (*6*). The as-isolated enzyme is virtually inactive unless Co (or Mn), but not Zn, is included in the assay medium, and this is thought to result in the addition of a second Co(II) (or Mn(II)) atom to the active site (*6*). The discovery that the metal atoms in the crystalline enzyme were not Co but Zn was a consequence of the method that was used to solve the structure. In the MAD method, the unequivocal identification of the metal in the crystals is a prerequisite of the experimental strategy. Had we chosen to solve the structure of *Pf*prol by, for example, molecular replacement or multiple isomorphous replacement, then in all probability the atoms

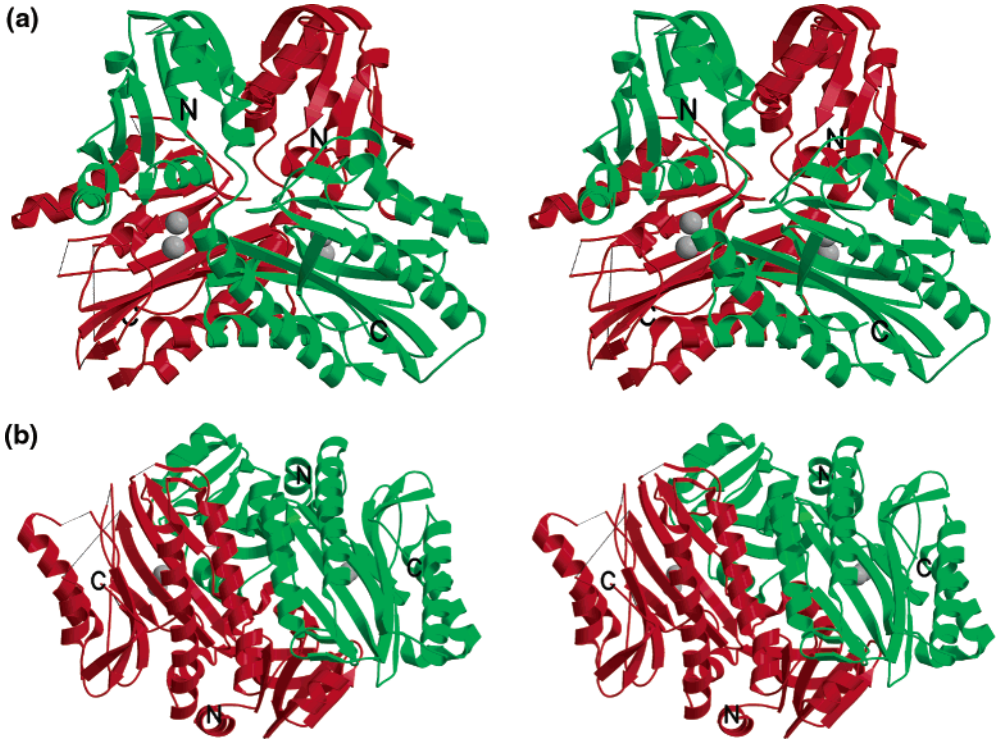

FIGURE 2: Stereoviews of the dimer of *Pf*prol. The subunits A and B are colored green and red, respectively. Portions of the protein backbone not refined in the model are indicated by dashed gray lines. (a) View with the local 2-fold axis lying vertically in the plane of the paper. The protein is illustrated as a ribbon to emphasize the secondary structure. (b) View looking along the 2-fold axis.

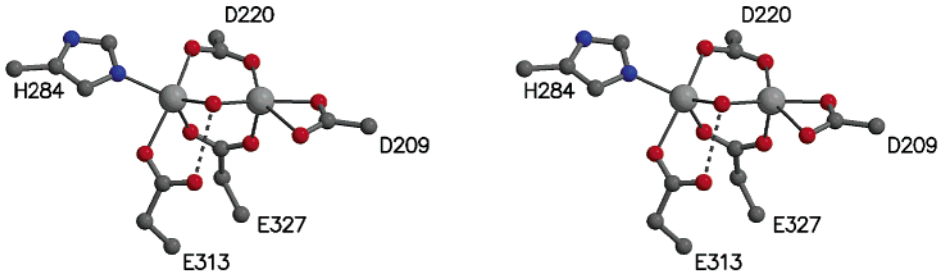

FIGURE 3: Stereoview showing the active site of *Pf*prol. The zinc atoms are shown as gray spheres. A hydrogen bond between Glu 313 and the bridging hydroxide ion is shown as a dotted line.

Table 2: Comparisons of the Zn−Ligand Distances in *Pf*prol with the Co−Ligand Distances in MetAP and the Mn−L Distances in APPro[a]

donor atom L	$d(Zn_A-L)$, Å in *Pf*prol[b]	$d(Zn_B-L)$, Å in *Pf*prol[b]	d(Co−L), Å in MetAP[c]	d(Mn−L), Å in APPro[d]
Asp209 $O^{\delta 1}$		2.1	2.1 (Asp97)	2.1 (Asp 260)
Asp209 $O^{\delta 2}$		2.8	2.4 (Asp97)	2.4 (Asp 260)
Asp220 $O^{\delta 1}$		2.0	2.0 (Asp108)	2.1 (Asp 271)
Asp220 $O^{\delta 2}$	2.2		1.9 (Asp108)	2.1 (Asp 271)
His284 $N^{\epsilon 2}$	2.1		2.2 (His171)	2.2 (His 354)
Glu313 $O^{\epsilon 2}$	2.3		2.1 (Glu204)	2.2 (Glu 383)
Glu327 $O^{\epsilon 1}$		2.0	2.2 (Glu235)	2.2 (Glu 406)
Glu 327 $O^{\epsilon 2}$	2.1		2.0 (Glu235)	2.2 (Glu 406)
solvent, W176	2.0	2.1	2.1, 2.1	2.1, 2.2
additional water				2.8, 2.4
Zn_A or Zn_B	3.1		3.2	3.3

[a] Estimated standard uncertainty of donor atom positions, calculated as the diffraction data precision indicator is 0.2 Å for *Pf*prol. The values for EcMetAP and EcAPPro are each approximately 0.1 Å, reflecting the higher resolution of these structure analyses (*46*). [b] Prolidase, molecule A at 2.0 Å resolution (PDB entry 1PV9) (present work). [c] EcMetAP at 1.9 Å resolution (PDB accession code 2MAT) (*38*). The metal atoms in EcMetAP are labeled Co1 and Co2, respectively; the ligands are shown in parentheses. The published coordinates for *Pf*MetAP (PDB accession number 1XGS (*18*) lead to similar values. [d] EcAPPro at 2.0 Å resolution (PDB accession code 1AZ9) (*13*).

at the active site would have been modeled incorrectly as Co. It is clear that the identity of the metal atoms in any metalloprotein crystal (and not just in the protein prior to crystallography) must be confirmed experimentally. X-ray absorption measurements currently offer the most direct and convenient means of doing so.

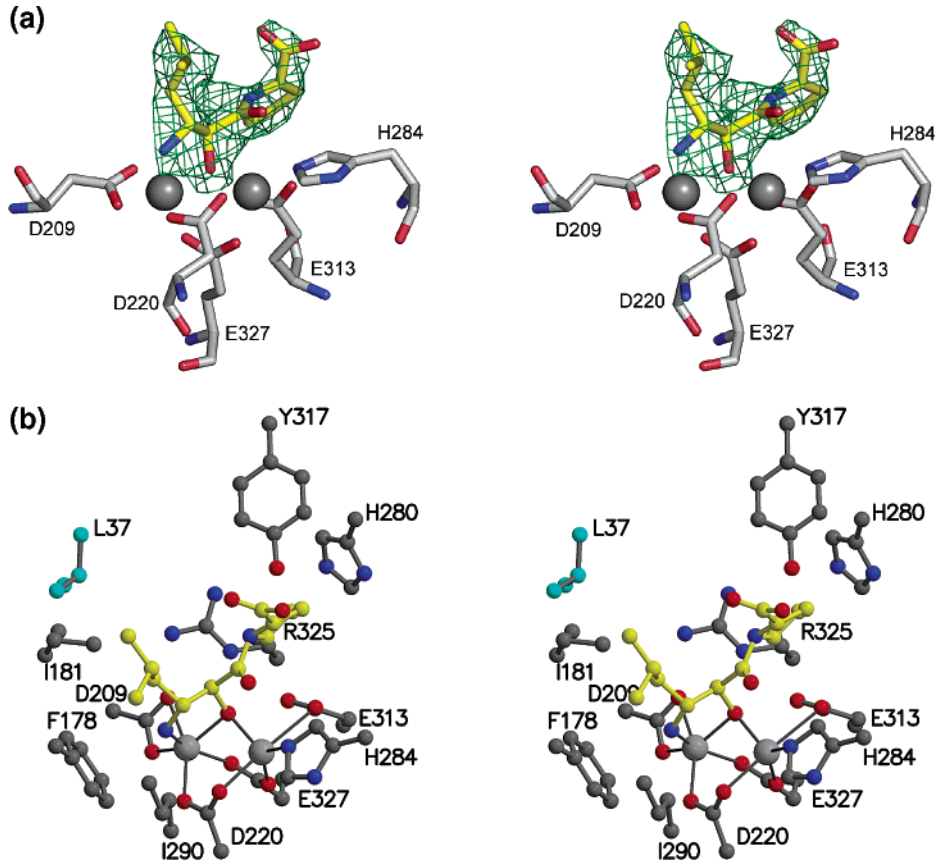

FIGURE 4: Stereoviews of the active site structure of *Pf*prol in complex with the AHMH-Pro inhibitor. (a) The Zn atoms are shown in metallic gray, with all five ligating amino acid residues (residue identities are indicated). Carbon atoms of the peptide are shown in gray and yellow in the inhibitor, oxygen atoms are in red, and nitrogen atoms are in blue. The difference Fourier electron density (contoured at 1.8σ) indicating the presence of the inhibitor is shown as a green net. The omit electron density was calculated at 2.3 Å resolution with no contribution from the inhibitor to the calculated structure factors. This figure was drawn with program PYMOL (*50*). (b) As in (a) but omitting the electron density but adding residues surrounding the inhibitor. The carbon atoms of residue Leu37 from the neighboring B subunit are colored cyan.

The Disorder in Subunit B. Despite the high resolution (2.0 Å) and good quality of the diffraction data (R_{merge} 0.035, Table 1), parts of the native *Pf*prol structure were found to be disordered. Several segments of subunit B had to be omitted from the final model since they were not associated with significant electron density and refinement led to unacceptably high temperature factors. These regions of the structure lack contacts to symmetry-related molecules in the crystal. For example, in subunit A the loop region comprising residues A227−A243 makes crystal contacts with residues A14−A16 in a symmetry-related molecule. The corresponding region in subunit B lacks such crystal contacts and is disordered (Supporting Information). Similar disorder was observed in a second crystal of the native protein (data not shown), and in the crystals of the AHMH-Pro complex (see below). We infer that the disorder is an inherent feature of the crystal form and not of an individual crystal.

This is not the first example of a homodimeric structure in which one subunit is seriously disordered. For instance, in the crystal structure of the transcription elongation/antitermination factor NusA from *Mycobacterium tuberculosis* at 1.7 Å resolution, the asymmetric unit contains two NusA molecules, each comprising an N-terminal and a C-terminal domain tethered by a seven-residue linker (*29*). The authors observed no interpretable electron density for the linker, and only one of the molecules in the asymmetric unit had well-defined electron density for the N-terminal domain. Apparently the N-terminal domain of the other molecule in the asymmetric unit was disordered. The fact that one of the N-terminal domains was ordered was ascribed to contacts qualitatively similar to those that we have observed in crystals of *Pf*prol.

Structural Comparisons with Related Proteins. As predicted from sequence similarities (*30*), a DALI search of the Protein Data Bank using the *Pf*prol coordinates (*31*) indicated that the proteins whose structures are most closely related to that of *Pf*prol are APPro from *E. coli* (PDB accession no. 1AZ9), the MetAPs from *E. coli* and *Homo sapiens* (PDB accession nos. 2MAT and 1BN5), and creatinase from *Pseudomonas putida* (PDB accession no. 1chm). Thus, *Pf*prol becomes a member of a group of enzymes whose most distinctive shared feature is a "pita-bread" fold of the C-terminal catalytic domain (*11*). *Pf*prol, APPro, and creatinase have, in addition, topologically similar N-terminal domains, but *E. coli* MetAP has no N-terminal domain, and human MetAP has a smaller nonhomologous N-terminal domain that is largely disordered in the crystals (*17*). The inclusion of creatinase is notable, since this enzyme has no metal atom at its active site, and is thought to use a protonated His side chain rather than a metal−ligand as the catalytically active group (*32*).

Table 3: Pairwise Comparisons among Aminopeptidase Structures rmsd between C^{α} Atom Positions in Superposed Domains, Å (and Number of C^{α} Atoms Included in the Superposition)[a]

	*Pf*prol	APPro	creatinase
*Pf*prol		2.0	1.7
	–	(71)	(101)
APPro	1.0		1.9
	(210)	–	(91)
creatinase	1.2	1.3	
	(211)	(210)	–
MetAP	1.3	1.2	1.4
	(198)	(187)	(171)

[a] Upper triangle: Pairwise superpositions of N-terminal domains. Lower triangle: Pairwise superpositions of C-terminal domains (or, in the case of *Ec*MetAP, the entire single-domain molecule). *Pf*prol, 2.0 Å resolution, PDB entry 1PV9 (present work); *Ec*APPro, 2.0 Å resolution, PDB entry 1AZ9 (*13*); *Ps. putida* creatinase, 1.9 Å resolution, PDB entry 1CHM (*32*); *Ec*MetAP, 1.9 Å resolution, PDB entry 2MAT (*38*). The calculations were made using LSQMAN (*47*).

Table 3 places the above comparisons on a quantitative basis. When a pair of N-terminal domains is superposed and C^{α} atoms in obviously nonequivalent positions are eliminated, the rmsd is consistently larger than when the C-terminal domains of the same proteins are superposed. The distance between the N- and C-terminal domains, and the orientation of one domain in relation to the other, also vary from protein to protein. This will be illustrated later for the specific case of *Pf*prol and APPro (see below, *Structural Reasons Why Prolidase Prefers Dipeptide Substrates*).

One consequence of the different organizations of the domains within the molecular monomers is that the states of aggregation in the crystal are different. In the crystal structures, MetAP exists as a monomer, *Pf*prol and creatinase are dimers, and APPro is a tetramer. These are also the quaternary structures of the enzymes in solution (*12, 13, 33*).

In contrast with MetAP, which has a different (or no) N-terminal domain, the observation that *Pf*prol is a dimer while APPro is a tetramer can be rationalized on the basis of the respective intersubunit contacts. APPro is a dimer of dimers (*13*). If the four monomeric subunits are labeled A, B, C, and D, then one dimer can be represented as A−B and the other as D−C. These two dimers are related by a crystallographic 2-fold axis. The contacts between the monomers within a dimer (e.g., between A and B) are different from the contacts between monomers in the symmetry-related dimers (e.g., between A and D). The buried surface area per subunit is 650 $Å^2$ in the contacts between A and B, and 2111 $Å^2$ in the contacts between A and D. The latter contacts occur in two regions of the molecular surface (*13*): (i) One contact region is formed by the intertwining of "arms" comprising residues 29A−49A and 29D−49D. One residue in the middle of the arm, Asp38D, is hydrogen-bonded to His361A at the active site of the neighboring monomer. (ii) A second contact region involves helices comprising residues 207A−222A and 207D−222D, some of which are linked by hydrogen bonds.

In the crystal structure of *Pf*prol, the contacts between the monomers A and B resemble some of the contacts between monomers A and D in APPro. The buried surface area is smaller (1525 $Å^2$ per monomer). As in APPro, there are hydrogen-bonded contacts between two helices comprising residues 158A−172A and 158B−172B, respectively (Supporting Information). However, there are no interactions in *Pf*prol comparable to those at residues 29−49A/D in APPro. Instead, a small additional contact region occurs at residues 92A−97A and 92B−97B, which form a short segment of antiparallel β-sheet. These differences between the monomer−monomer interfaces in *Pf*prol and APPro are associated with the different orientations of the N-terminal domain in relation to the C-terminal domain (see below). Aggregation of the *Pf*prol dimers into tetramers is prevented by the closer proximity of the N-terminal and C-terminal domains. This steric restraint is unlikely to be the result of forces in the crystal, since there is no evidence for tetramerization in solution. Indeed, in view of the hyperthermostable nature of *Pf*prol, for example, the native *Pf* enzyme shows no loss of activity after 12 h at 100 °C (*6*), much more enhanced subunit−subunit interactions compared to the mesophilic APPro (from *E. coli*) would have been anticipated. Thus, while this mechanism is thought to be key to the thermal stabilization of some enzymes from hyperthermophilic organisms (*34*), it is clearly not the case here. In addition, in detailed comparisons between high-resolution structures of hyperthermophilic proteins and their mesophilic counterparts the former generally have an increased number of salt bridges or hydrogen bonds and a decreased solvent exposed surface area (see for example ref *18*). No structure of a mesothermophilic prolidase has been solved making a detailed comparison impossible. However, we note that compared with *Ec*APPro the exposed loops in *Pf*prol appear to have been trimmed considerably (Figure 6).

The Dinuclear Zinc Site in Pfprol. The dinuclear Zn(II) site in *Pf*prol closely resembles the dinuclear Co(II) site in MetAP and the dinuclear Mn(II) site in APPro. Pairwise superpositions of the three active-site structures show that there is close agreement between the coordination geometries (Figure 5). In the superposition of the active sites of *Pf*prol and APPro, not only the ligand residues but also most of the next shell of surrounding residues occupy closely similar positions (Figure 5b).

The metal−ligand bonds in the three enzymes are compared in Table 2. In all three structures, the two metal atoms are bridged by two *syn*-bidentate carboxylate groups and a water molecule. (The latter is likely to act as a hydroxide ion at physiological pH.) In addition, one metal atom is coordinated by a monodentate carboxylate group and a His side chain, and the other is coordinated by a bidentate carboxylate group. Thus, both Zn(II) atoms in *Pf*prol and both Co(II) atoms in MetAP are five-coordinate. In APPro, one of the Mn(II) atoms is six-coordinate, the additional ligand being a solvent H_2O; the other Mn(II) atom is six-coordinate with a weak (2.8 Å) $Mn-OH_2$ bond in one crystal form (*13*) and five-coordinate in another (*35*). Within the limits of precision, the Zn−Zn distance in *Pf*prol (3.1 Å), the Co−Co distance in MetAP (3.2 Å), and the Mn−Mn distance in APPro (3.3 Å) are not significantly different.

The coordination sphere of one metal atom at each dinuclear site includes the side chain carboxylate group of an Asp as a bidentate ligand. In *Pf*prol, the bidentate coordination is markedly unsymmetrical, the Zn_B-O(carboxylate) bond lengths being 2.1 and 2.8 Å, respectively. The differences between the corresponding Co−O(carboxylate) bonds in MetAP and between the corresponding Mn−O(carboxylate) bonds in APPro are slightly smaller (2.1 and

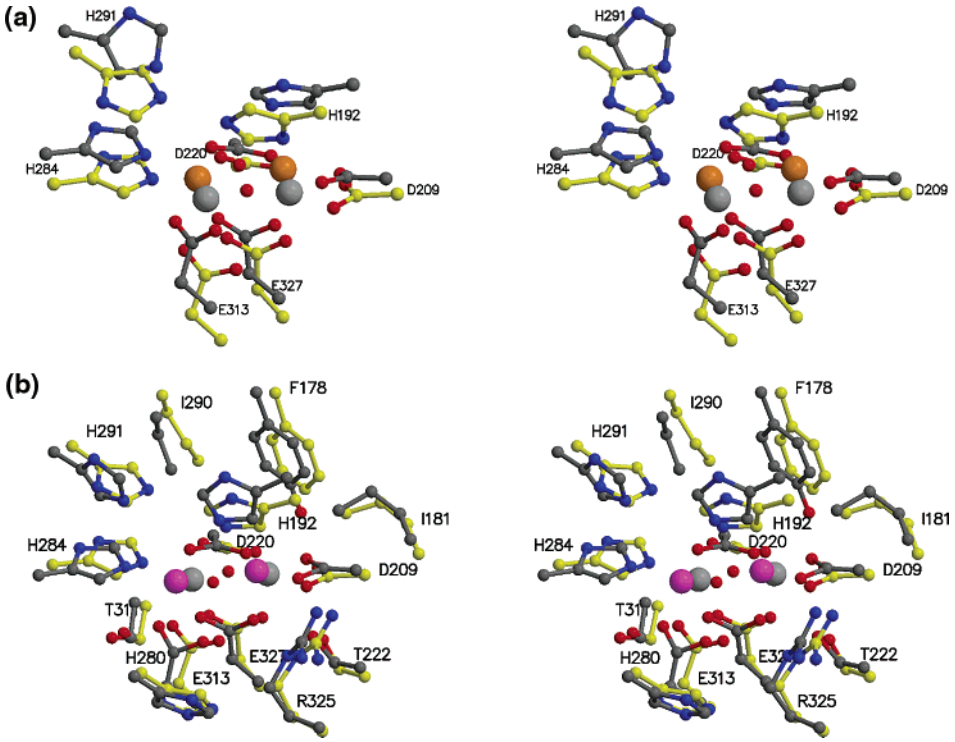

FIGURE 5: Stereoviews showing the superposition of the active sites of *Pf*prol and related enzymes. The sites have been displaced to enhance the clarity of the view. The metal ligand and surrounding residues are shown. (a) *Pf*prol (gray bonds) and MetAP (yellow bonds). The metal atoms are shown as spheres. Zn in *Pf*prol gray and Co in MetAP orange. (b) *Pf*prol (gray bonds) and APPro (yellow bonds). The metal atoms are shown as spheres. Zn in *Pf*prol is gray and Mn in APPro is magenta.

2.4 Å in both proteins). The tendency of carboxylate groups to act as unsymmetrical bidentate ligands is well-known in model compounds of Zn(II) and other metals (*36*).

Why Is the Zinc-Substituted Form of P. furiosus Prolidase Inactive? Most of the known metallopeptidases with dinuclear metal centers have been identified as Zn enzymes (*37*). Thus, the three "pita-bread" metallopeptidases compared in the present work, two di-Co(II) enzymes and a di-Mn(II) enzyme, appear to belong to a minority. Without knowing what the essential features of a zinc enzyme are, we note that in *Pf*prol and in APPro substitution with zinc leads to a metal site with different ligands to any naturally occurring authentic zinc enzyme. The effectiveness of Zn(II) in the enzymatic catalysis of hydrolytic, condensation, and other atom- or group-transfer reactions can be explained on the grounds of its flexible four-, five-, and six-coordination geometry, fast ligand exchange, Lewis acidity, intermediate hard−soft character, bioavailability, strong binding to suitable ligands, and lack of redox activity (*37*). These qualities are not unique to Zn(II) (d^{10}), and with obvious reservations apply also to other metals such as high-spin Mn(II) (d^5) and Co(II) (d^7). It is therefore not surprising that the activity of many Zn enzymes is maintained or even enhanced when the active-site Zn(II) is replaced by other metals such as Mn(II) and Co(II). For example, the metallopeptidases *b*LeuAP, *Ap*AP, and *Sg*AP all remain active when their di-Zn(II) active site is replaced by Co(II) (*11*). What is surprising is that the converse, the replacement of Co(II) or Mn(II) by Zn(II), deactivates at least two of the three peptidases that we have been comparing.

As a working hypothesis, we assume that the di-Zn(II)-substituted *Pf*prol, whose structure is reported here, is isostructural with native di-Co(II) *Pf*prol. If this is correct, then the di-Co(II) site in native *Pf*prol, the di-Co(II) site in MetAP, and the di-Mn(II) site in APPro all have closely similar structures. All three sites are catalytically active, but *Pf*prol and APPro become inactive when the metal atoms in the native enzyme are replaced by Zn(II). The reasons for this are not yet clear, and there is a possibility that further studies will lead to unexpected explanations. This is illustrated by the sequential reinterpretations of the metal-dependence of *E. coli* MetAP. The enzyme was originally reported to require two Co(II) atoms per molecule for full activity. The Zn(II)-loaded enzyme had a lower but significant activity (*38*). The highest activity was later recorded for the enzyme in the presence of one Fe(II) atom per molecule (*39*). The most recent evidence suggests that *E. coli* MetAP functions best with only one Fe(II) or Co(II) atom, and that it may function as a mononuclear enzyme in vivo (*40*).

A Basis for Prolidase Inhibition. The inhibitor AHMH-Pro is 3*R*-amino-2*S*-hydroxy-5-methyl-hexanoyl-proline, or a dipeptide with one β amino acid (β3-Leu-Pro) with a hydroxyl substituent on the 2- or α-position of Leu. It is a potent inhibitor of porcine kidney prolidase with $K_i = 16$ nM (cited by Maggiora et al. (*41*)). If we assume that the interaction of the inhibitor with Zn(II)-loaded *Pf*prol correctly models the interaction with the native protein, then three features of the inhibitor−protein complex appear to be mechanistically relevant. The NH_2-group of the inhibitor ligates the active-site Zn_A atom; His192 and His291 of the enzyme form hydrogen bonds with the terminal carboxylate group and the O(peptide) of the inhibitor, respectively; and the -OH group of the inhibitor bridges the two Zn(II) atoms.

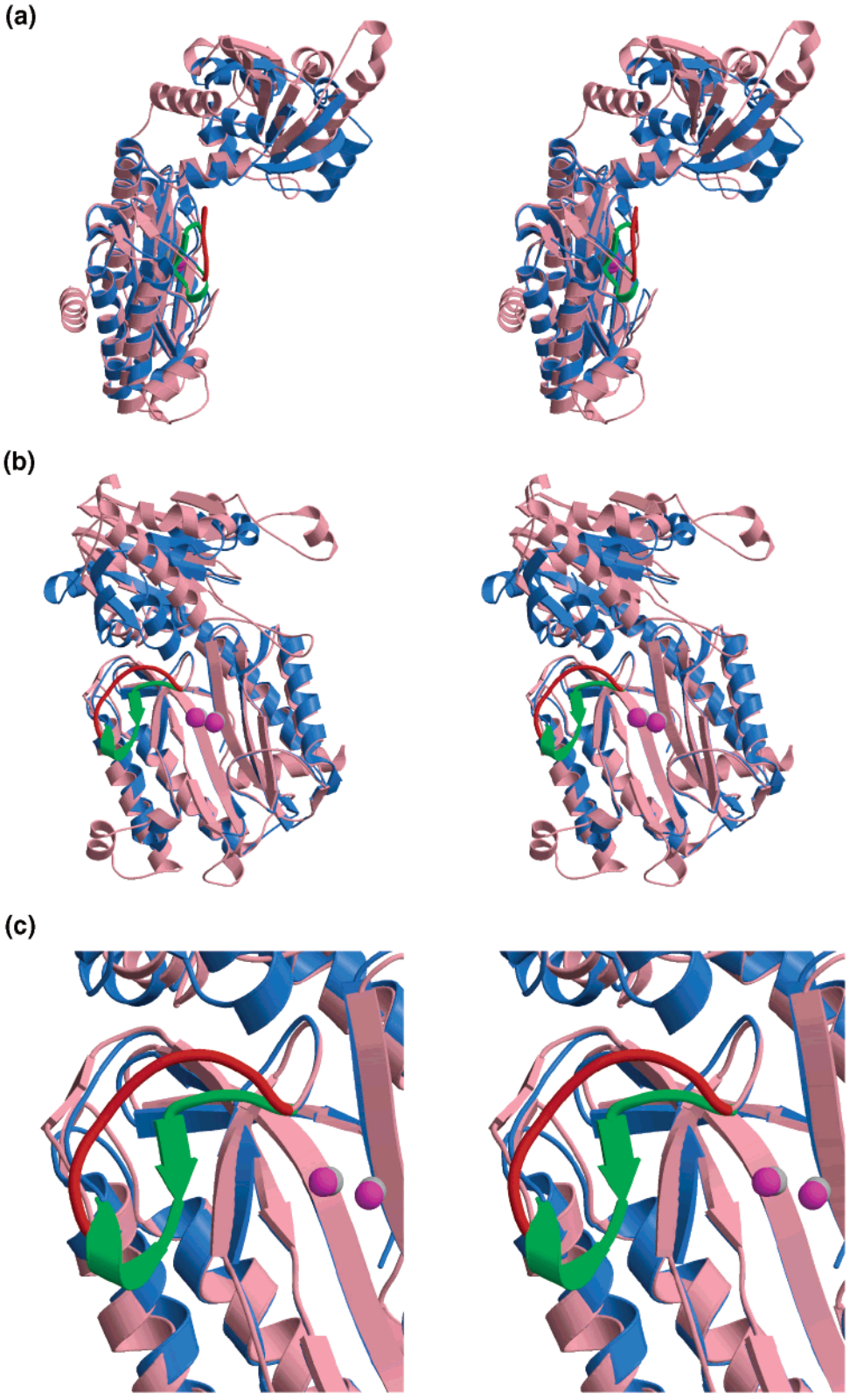

FIGURE 6: Stereodiagrams showing a superposition of the monomeric subunits of *Pf*prol (blue) and APPro (pink). Only 210 residues in the C-terminal domain of each monomer were included in the superposition. The lower part of each diagram shows clearly that the C-terminal domains of the two molecules have strong structural homology. In the upper part of each diagram, the N-terminal domains are seen to have significantly different orientations with respect to the C-terminal domains. In *Pf*prol, a loop (residues 291−300) that folds down toward the active site is highlighted in green. The equivalent residues in APPro (361−369) are colored red. It is suggested that the proximity of this loop to the dinuclear metal site in *Pf*prol accounts for the preferences of the enzyme for dipeptide substrates (see text). In (b), the molecules are rotated by 90° about the vertical axis with respect to their orientation in (a). The metal atoms are represented as spheres (gray, Zn; magenta, Mn). (c) Shows an enlarged view of the highlighted loops and the active site in the same orientation as (b).

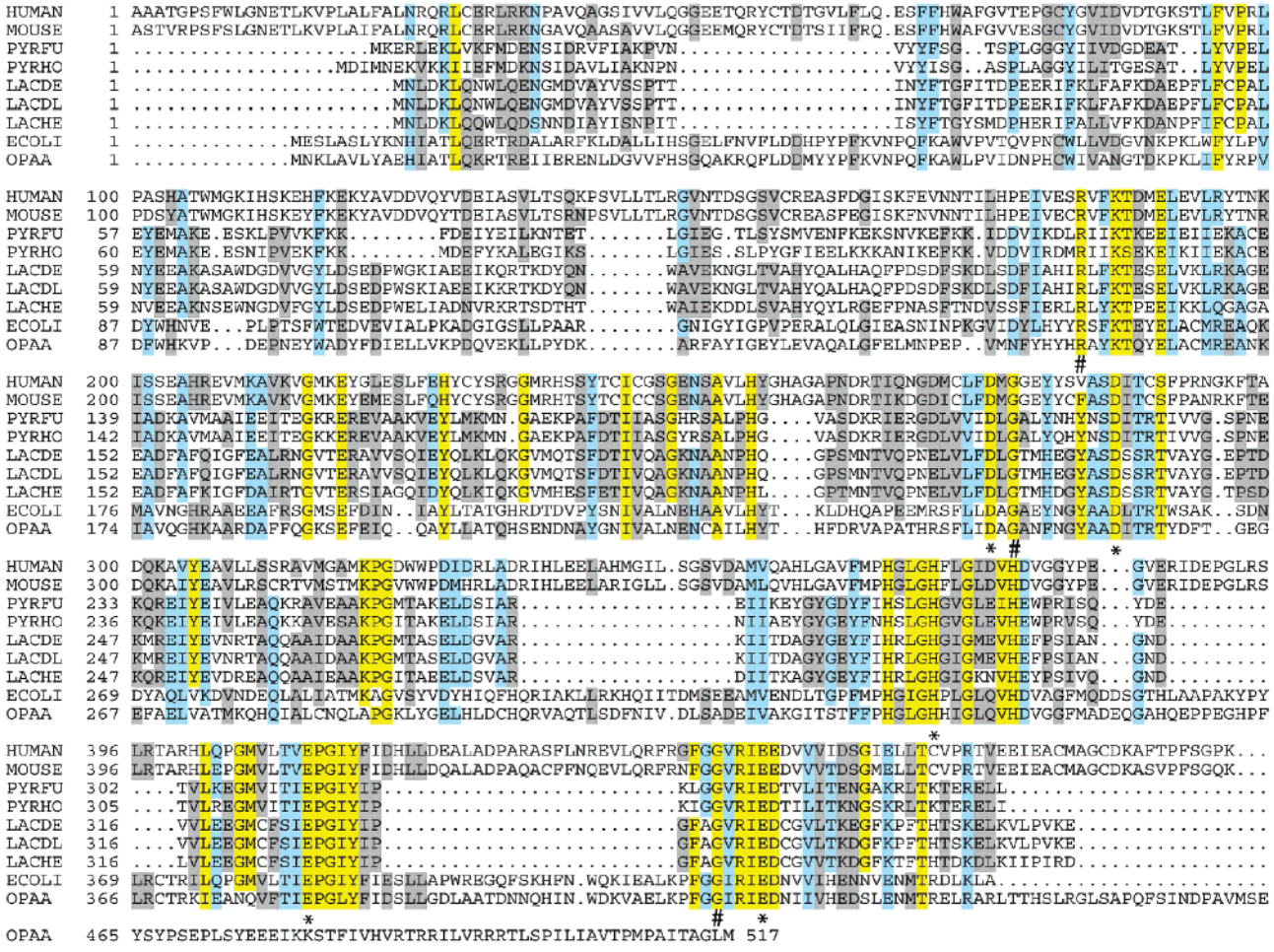

FIGURE 7: Alignment of prolidase and OPAA sequences. Abbreviations are as follows: HUMAN, *homo sapiens*, accession code P12955; MOUSE, *Mus Musculus*, Q11136; PYRFU, *Pyrococcus furiosus*, P81535; PYRHO, *Pyrococcus horikoshii*, O58885; LACDE, *Lactobacillus delbrueckii subsp. bulgarious*, Q95651; LACDL, *Lactobacillus delbrueckii subsp. lactis*, P46545; LACHE, *Lactobacillus helveticus*, O84913; ECOLI, *Escherichia coli*, P21165; OPAA, Organophosphorus acid anhydrolase-2, *Alteromonas sp*., Q44238. Residues that ligate the dinuclear metal site are marked as *; three of the four residues, where mutations are associated with prolidase deficiency in humans, are marked as #. Asp 220 is both a metal ligand and the site of a deficiency-associated mutation, and is marked only as *. Regions of high sequence similarity are shaded yellow. Regions with less similarity are shaded blue and gray.

The first observation is consistent with a suggestion that metal-NH_2 binding helps to determine the specificity of the enzyme for cleavage of the N-terminal residue (*11*); the second observation has not, to the best of our knowledge, been implicated in a reaction mechanism; and the displacement of the bridging hydroxide group probably provides the main basis for inhibition. The same displacement of the bridging hydroxide group from a di-Zn(II) site has been observed in inhibitor complexes of three other metallopeptidases, namely, the amastatin and l-leucinal complexes of *b*LeuAP (*42*, *43*), the *p*-iodo-D-phenylalanine-hydroxamate complex of *Ap*AP (*44*), and a (3*R*,2*S*)-3-amino-2-hydroxyheptanoyl-L-Ala-L-Leu- L-Val-L-Phe-OMe complex of MetAP (*38*).

Structural Reasons Why Prolidase Prefers Dipeptide Substrates. In discussing the states of aggregation of *Pf*prol and APPro, we have referred to the pronounced differences between the structures of the monomers. When the monomers are superposed using only the C-terminal domains, the N-terminal domains overlay poorly (Figure 6). While the domain topologies are similar, the angles between the N- and C-terminal domains are different. Further, the helix comprising residues 113−123 in *Pf*prol, which links the two domains, lies at a more acute angle with respect to the C-terminal domain than the equivalent helix in APPro (residues 164−174). Consistent with the different position of the helix, the N-terminal domain in *Pf*prol lies closer to the C-terminal domain than in APPro, and a loop at residues 291−300 in *Pf*prol has a different structure and approaches the active site more closely than the corresponding region in APPro (residues 361−369). The active site in *Pf*prol is further crowded by parts of the N-terminal domain of the neighboring subunit (residues 36B−39B). The potential effect of this crowding becomes apparent when *Pf*prol is superposed on a complex of APPro with Pro−Leu, an inhibitor that resembles the hydrolysis product of that enzyme (*13*). In the superposed structures, *Pf*prol residues A294−A296 and B36−B39 lie close (3−7 Å) to the C-terminal residue of the inhibitor in APPro. We propose that these two polypeptide segments in *Pf*prol provide the means for inhibiting the binding of peptides longer than two residues.

The structure of the *Pf*prol dimer is replicated within close limits in creatinase (Table 3). The relationship between the domains within the subunits of the two enzymes is also

similar. Like *Pf*prol, creatinase acts on relatively small substrates, and access of larger substrates is prevented by a polypeptide loop similar to that in *Pf*prol.

Other features of *Pf*prol that may contribute to the preference for particular dipeptide substrates are suggested by further comparisons with APPro and with MetAP−inhibitor complexes. We use the same nomenclature as Lowther and Matthews (*11*), who label the N-terminal residue of a peptide P_1, and the adjacent residue P_1'. The preferred substrates of prolidase are dipeptides with a nonpolar residue at P_1 (Met, Leu, Val, Phe, Ala) and a *trans*-Pro at P_1'. APPro requires oligopeptide substrates with a hydrophobic or basic residue in the P_1 position and a *trans*-Pro at P_1'. MetAPs require a Met residue at P_1 and a small, uncharged residue at P_1' (Gly, Ala, Ser, Thr, Val, Pro, Cys) (*11*). These preferences must be reflected in the structures.

The P_1 binding site in *Pf*prol is lined by hydrophobic residues Ile181, Phe178, Ile290, and by Leu37B in the neighboring subunit (Figure 4b). The comparable residues in APPro are Ile232, Tyr229, and Val360, respectively. An interaction with a residue comparable to Leu37B is missing, since the structures of the two enzymes in this region are different (see above). The presence of the polar Tyr, Asp, and Ser residues in APPro may explain its ability to function on substrates with basic residues in the P_1 position, whereas prolidase requires a nonpolar residue. The equivalent P_1 binding pocket in MetAP is bordered by Cys70, Cys59, and Phe177, providing the specificity for a Met residue in this position. In *Pf*prol and APPro, the Pro (P_1') binding pocket is lined by identical residues: His280 (350, APPro), Tyr317 (387, APPro), and Arg325 (404, APPro). His280 makes a van der Waals contact with the AHMH-Pro P_1' residue (His280 ND1-Pro CG = 3.5 Å). The interactions do not appear to be tight enough to explain the strict requirement for Pro in this position.

The Molecular Basis of "Prolidase Deficiency". Mutations in the gene encoding human prolidase cause prolidase deficiency, an autosomal recessive disorder mainly characterized by skin lesions, mental retardation, and recurrent infections. A search of the Human Gene Mutation database (*45*) reveals four point mutations in human prolidase that have been identified in patients with this disorder: mutation 1, Arg184Gln (Arg122Gln in *Pf*prol); mutation 2, Asp276Asn (Asp209Asn in *Pf*prol); mutation 3, Gly278Asp (Gly211Asp in *Pf*prol); and mutation 4, Gly448Arg (Gly323Arg in *Pf*prol). The mutated residues are conserved in all other known prolidase sequences and in OPAA (Figure 7). Mapping of the mutations on the structure of *Pf*prol leads to the following observations.

(i) Arg122 lies on the helix linking the N- and C-terminal domains, and participates in a salt bridge with Glu289 (see table in Supporting Information). An Arg → Gln mutation (mutation 1) presumably disrupts this interaction between the linker and domain II. The potential effects of this disruption on the molecular structure are still to be explored. (ii) Asp209 is a ligand to Zn_B. Mutation to Asn (mutation 2) would replace the coordinating -COO^- group with a neutral -$CONH_2$ group. Possible consequences are a weakening or loss of the Zn_B−ligand bond, and a change from a dinuclear to a mononuclear metal site with a lower catalytic activity. (iii) The C^α atom of Gly211 makes a close contact with the O(carbonyl) atom of Ser219 in a neighboring β-strand. When -H in Gly211 is replaced by a bulkier side chain (mutation 3), the resulting movement of Ser219 is likely to be transmitted to its neighbor in the β-strand, namely, the metal ligand Asp220. (iv) In a similar fashion, a close contact between the C^α atom of Gly323 and the O(carbonyl) atom of Ile316 implies that a Gly → Arg change at Gly323 (mutation 4) will force Ile316 to move. This movement may affect other residues on the same β-strand, including the metal-binding residue Glu313.

ACKNOWLEDGMENT

We thank Professor William Simmons of Loyola University for providing the AHMH-Pro inhibitor and for helpful discussion, Dr. Barry Fields and Dr. Paul Ellis for assistance at the synchrotron with data collection, and Dr. Frank Jenney for help with the metal analyses.

SUPPORTING INFORMATION AVAILABLE

A table giving details of the interdomain, intersubunit, and intermolecular contacts in the crystal structure of *P. furiosus* prolidase is available free of charge via the Internet at http://pubs.acs.org.

REFERENCES

1. Browne, P., and O'Cuinn, G. (1983) The purification and characterization of a proline dipeptidase from guinea pig brain. *J. Biol. Chem. 258*, 6147−54.
2. Endo, F., Tanoue, A., Nakai, H., Hata, A., Indo, Y., Titani, K., and Matsuda, I. (1989) Primary structure and gene localization of human prolidase. *J. Biol. Chem. 264*, 4476−81.
3. Sjostrom, H., Noren, O., and Josefsson, L. (1973) Purification and specificity of pig intestinal prolidase. *Biochim. Biophys. Acta 327*, 457−70.
4. Fernandez-Espla, M. D., Martin-Hernandez, M. C., and Fox, P. F. (1997) Purification and characterization of a prolidase from *Lactobacillus casei* subsp. *casei* IFPL 731. *Appl. Environ. Microbiol. 63*, 314−6.
5. Suga, K., Kabashima, T., Ito, K., Tsuru, D., Okamura, H., Kataoka, J., and Yoshimoto, T. (1995) Prolidase from *Xanthomonas maltophilia*: purification and characterization of the enzyme. *Biosci. Biotechnol. Biochem. 59*, 2087−90.
6. Ghosh, M., Grunden, A. M., Dunn, D. M., Weiss, R., and Adams, M. W. (1998) Characterization of native and recombinant forms of an unusual cobalt-dependent proline dipeptidase (prolidase) from the hyperthermophilic archaeon *Pyrococcus furiosus*. *J. Bacteriol. 180*, 4781−9.
7. Forlino, A., Lupi, A., Vaghi, P., Icaro Cornaglia, A., Calligaro, A., Campari, E., and Cetta, G. (2002) Mutation analysis of five new patients affected by prolidase deficiency: the lack of enzyme activity causes necrosis-like cell death in cultured fibroblasts. *Hum. Genet. 111*, 314−22.
8. Endo, F., Tanoue, A., Hata, A., Kitano, A., and Matsuda, I. (1989) Deduced amino acid sequence of human prolidase and molecular analyses of prolidase deficiency. *J. Inherited Metab. Disease 12*, 351−4.
9. Bockelmann, W. (1995) The proteolytic system of starter and nonstarter bacteria: components and their importance for cheese ripening. *Int. Dairy J. 5*, 977−94.
10. Cheng, T. C., Harvey, S. P., and Chen, G. L. (1996) Cloning and expression of a gene encoding a bacterial enzyme for decontamination of organophosphorus nerve agents and nucleotide sequence of the enzyme. *Appl. Environ. Microbiol. 62*, 1636−41.
11. Lowther, W. T., and Matthews, B. W. (2002) Metalloaminopeptidases: common functional themes in disparate structural surroundings. *Chem. Rev. 102*, 4581−607.
12. Roderick, S. L., and Matthews, B. W. (1993) Structure of the cobalt-dependent methionine aminopeptidase from *Escherichia coli*: a new type of proteolytic enzyme. *Biochemistry 32*, 3907−12.
13. Wilce, M. C. J., Bond, C. S., Dixon, N. E., Freeman, H. C., Guss, J. M., Lilley, P. E., and Wilce, J. A. (1998) Structure and

mechanism of a proline-specific aminopeptidase from *Escherichia coli*. *Proc. Natl. Acad. Sci., U.S.A. 95*, 3472−77.
14. Strater, N., and Lipscomb, W. N. (1995) Transition state analogue L-leucinephosphonic acid bound to bovine lens leucine aminopeptidase: X-ray structure at 1.65 Å resolution in a new crystal form. *Biochemistry 34*, 9200−10.
15. Chevrier, B., Schalk, C., D'Orchymont, H., Rondeau, J. M., Moras, D., and Tarnus, C. (1994) Crystal structure of *Aeromonas proteolytica* aminopeptidase: a prototypical member of the co-catalytic zinc enzyme family. *Structure 2*, 283−91.
16. Gilboa, R., Spungin-Bialik, A., Wohlfahrt, G., Schomburg, D., Blumberg, S., and Shoham, G. (2001) Interactions of *Streptomyces griseus* aminopeptidase with amino acid reaction products and their implications toward a catalytic mechanism. *Proteins 44*, 490−504.
17. Liu, S., Widom, J., Kemp, C. W., Crews, C. M., and Clardy, J. (1998) Structure of human methionine aminopeptidase-2 complexed with fumagillin. *Science 282*, 1324−7.
18. Tahirov, T. H., Oki, H., Tsukihara, T., Ogasahara, K., Yutani, K., Ogata, K., Izu, Y., Tsunasawa, S., and Kato, I. (1998) Crystal structure of methionine aminopeptidase from hyperthermophile, *Pyrococcus furiosus*. *J. Mol. Biol. 284*, 101−24.
19. Rowsell, S., Pauptit, R. A., Tucker, A. D., Melton, R. G., Blow, D. M., and Brick, P. (1997) Crystal structure of carboxypeptidase G2, a bacterial enzyme with applications in cancer therapy. *Structure 5*, 337−47.
20. Willingham, K., Maher, M. J., Grunden, A. M., Ghosh, M., Adams, M. W., Freeman, H. C., and Guss, J. M. (2001) Crystallization and characterization of the prolidase from *Pyrococcus furiosus*. *Acta Crystallogr., Sect. D: Biol. Crystallogr. 57*, 428−30.
21. Otwinowski, Z., and Minor, W. (1997) Processing of X-ray Diffraction Data Collected in Oscillation Mode. *Methods Enzymol. 276*, 307−26.
22. Brunger, A. T., Adams, P. D., Clore, G. M., Delano, W. L., Gros, P., Grossekunstleve, R. W., Jiang, J. S., Kuszewski, J., Nilges, M., Pannu, N. S., Read, R. J., Rice, L. M., Simonson, T., and Warren, G. L. (1998) Crystallography and NMR system − a new software suite for macromolecular structure determination. *Acta Crystallogr., Sect. D: Biol. Crystallogr. 54*, 905−21.
23. CCP4. (1994) Collaborative Computational Project no. 4. *Acta Crystallogr., Sect D: Biol. Crystallogr. 50*, 760−3.
24. Cowtan, K. D., and Zhang, K. Y. (1999) Density modification for macromolecular phase improvement. *Prog. Biophys. Mol. Biol. 72*, 245−70.
25. Jones, T. A., Zou, J.-Y., Cowan, S. W., and Kjeldgaard, M. (1991) Improved methods for building protein models in electron density maps and the location of errors in these models. *Acta Crystallogr., Sect. A 47*, 110−9.
26. Murshudov, G. N., Vagin, A. A., and Dodson, E. J. (1997) Refinement of macromolecular structures by the maximum-likelihood methodology. *Acta Crystallogr., Sect. D: Crystallogr. 53*, 240−55.
27. Jones, S., and Thornton, J. M. (1997) Prediction of protein−protein interaction sites using patch analysis. *J. Mol. Biol. 272*, 121−32.
28. Suda, H., Aoyagi, T., Takeuchi, T., and Umezawa, H. (1976) Inhibition of aminopeptidase B and leucine aminopeptidase by bestatin and its stereoisomer. *Arch. Bioch. Biophys. 177*, 196−200.
29. Gopal, B., Haire, L. F., Gamblin, S. J., Dodson, E. J., Lane, A. N., Papavinasasundaram, K. G., Colston, M. J., and Dodson, G. (2001) Crystal structure of the transcription elongation/anti-termination factor NusA from *Mycobacterium tuberculosis* at 1.7 Å resolution. *J. Mol. Biol. 314*, 1087−95.
30. Bazan, J. F., Weaver, L. H., Roderick, S. L., Huber, R., and Matthews, B. W. (1994) Sequence and structure comparison suggest that methionine aminopeptidase, prolidase, aminopeptidase P, and creatinase share a common fold. *Proc. Natl. Acad. Sci., U.S.A. 91*, 2473−77.
31. Holm, L., and Sander, C. (1993) Protein structure comparison by alignment of distance matches. *J. Mol. Biol. 233*, 123−38.
32. Coll, M., Knof, S. H., Ohga, Y., Messerschmidt, A., and Huber, R. (1990) Enzymatic mechanism of creatine amidinohydrolase as deduced from crystal structures. *J. Mol. Biol. 214*, 597−610.
33. Hoeffken, H. W., Knof, S. H., Bartlett, P. A., and Huber, R. (1988) Crystal structure determination, refinement and molecular model of creatine amidinohydrolase from *Pseudomonas putida*. *J. Mol. Biol. 204*, 417−33.
34. Clantin, B., Tricot, C., Lonhienne, T., Stalon, V., and Villeret, V. (2001) Probing the role of oligomerization in the high thermal stability of Pyrococcus furiosus ornithine carbamoyltransferase by site-specific mutants. *Eur. J. Biochem. 268*, 3937−42.
35. Graham, S. C., Lee, M., Freeman, H. C., and Guss, J. M. (2003) An orthorhombic form of *Escherichia coli* aminopeptidase P at 2.4 Å resolution. *Acta Crystallogr., Sect. D: Biol. Crystallogr. 59*, 897−902.
36. Freeman, H. C. (1973) in *Inorganic Biochemistry* (Eichorn, G., Ed.) pp 121−166, Elsevier, Amsterdam.
37. Lipscomb, W. N., and Strater, N. (1996) Recent advances in zinc enzymology. *Chem. Rev. 96*, 2375−433.
38. Lowther, W. T., Orville, A. M., Madden, D. T., Lim, S., Rich, D. H., and Matthews, B. W. (1999) *Escherichia coli* methionine aminopeptidase: implications of crystallographic analyses of the native, mutant, and inhibited enzymes for the mechanism of catalysis. *Biochemistry 38*, 7678−88.
39. D'Souza V. M., and Holz, R. C. (1999) The methionyl aminopeptidase from *Escherichia coli* can function as an iron(II) enzyme. *Biochemistry 38*, 11079−85.
40. D'Souza V. M., Bennett, B., Copik, A. J., and Holz, R. C. (2000) Divalent metal binding properties of the methionyl aminopeptidase from *Escherichia coli*. *Biochemistry 39*, 3817−26.
41. Maggiora, L. L., Orawski, A. T., and Simmons, W. H. (1999) Apstatin analogue inhibitors of aminopeptidase P, a bradykinin-degrading enzyme. *J. Med. Chem. 42*, 2394−402.
42. Strater, N., and Lipscomb, W. N. (1995) Two-metal ion mechanism of bovine lens leucine aminopeptidase: active site solvent structure and binding mode of L-leucinal, a gem-diolate transition state analogue, by X-ray crystallography. *Biochemistry 34*, 14792−800.
43. Kim, H., and Lipscomb, W. N. (1993) X-ray crystallographic determination of the structure of bovine lens leucine aminopeptidase complexed with amastatin: formulation of a catalytic mechanism featuring a gem-diolate transition state. *Biochemistry 32*, 8465−78.
44. Chevrier, B., D'Orchymont, H., Schalk, C., Tarnus, C., and Moras, D. (1996) The structure of the *Aeromonas proteolytica* aminopeptidase complexed with a hydroxamate inhibitor. Involvement in catalysis of Glu151 and two zinc ions of the co-catalytic unit. *Eur. J. Biochem. 237*, 393−8.
45. Krawczak, M., and Cooper, D. N. (1997) The human gene mutation database. *Trends Genet. 13*, 121−2.
46. Cruickshank, D. W. J. (1999) Remarks about protein structure precision. *Acta Crystallogr., Sect. D: Biol. Crystallogr. 55*, 583−601.
47. Kleywegt, G. J., and Jones, T. A. (1995) Where freedom is given, liberties are taken. *Structure 3*, 535−40.
48. Kraulis, P. J. (1991) MOLSCRIPT: a program to produce both detailed and schematic plots of protein structure. *J. Appl. Crystallogr. 24*, 946−950.
49. Merritt, E. A., and Murphy, M. E. P. (1994) RASTER3D version 2.0: a program for photorealistic molecular graphics. *Acta Crystallogr., Sect. D: Biol. Crystallogr. 50*, 869−73.
50. Delano, W. L. (2002) PYMOL, Delano Scientific, San Carlos, CA.

BI0356451